J. Fluid Mech. (2009), *vol.* 627, *pp.* 403–421. © 2009 Cambridge University Press
doi:10.1017/S0022112009005783 Printed in the United Kingdom

Mean induction and diffusion: the influence of spatial coherence

ALICE COURVOISIER,† DAVID W. HUGHES AND STEVEN M. TOBIAS

Department of Applied Mathematics, University of Leeds, Leeds LS2 9JT, UK

(Received 6 September 2008 and in revised form 17 December 2008)

Within the same framework we calculate the mean induction of a magnetic field and the mean diffusivity of a passive scalar, for two families of flows in which the degree of spatial decorrelation can be systematically adjusted. We investigate the dependence of these quantities both on the spatial decoherence and on the molecular diffusivity. We demonstrate that for flows with similar global properties, the mean induction is dramatically reduced as the flows become less spatially correlated; the mean diffusivity, on the other hand, shows no significant or systematic variation.

1. Introduction

Turbulent flows are typically characterized by the presence of a wide range of spatial and temporal scales. In many situations one is interested in the evolution of large-scale, or mean, quantities, for which it is necessary to parameterize the effects of the small scales. Clearly this involves the notion of an averaging procedure, which may be performed in a number of different ways – for example, spatially, temporally or by means of ensemble averages. The interpretation of the various types of average is, however, far from straightforward; it is the aim of this paper to explore one of the subtle issues that arises in this context.

Different large-scale quantities can be of interest, depending on the particular problem under consideration; for example, linear momentum in channel or pipe flow, angular momentum in rotating turbulence, the heat flux in convective turbulence, a scalar contaminant in environmental flows and the electromotive force (e.m.f.) in magnetohydrodynamic (MHD) turbulence. In this paper we shall investigate the evolution of two of these large-scale quantities, namely the e.m.f. in MHD turbulence, and the flux of a passive scalar.

At the heart of the mean field formulation of turbulence is the expression of interactions between small-scale quantities in terms of large-scale quantities and their spatial derivatives.‡ For example, for a passive scalar C in a turbulent velocity field $\boldsymbol{u}(\boldsymbol{x}, t)$ one may express the mean flux $\overline{\boldsymbol{u}c}$ as

$$F_i \equiv \overline{u_i c} = -D_{ij}\frac{\partial \overline{C}}{\partial x_j} - E_{ijk}\frac{\partial^2 \overline{C}}{\partial x_j \partial x_k} + \cdots, \tag{1.1}$$

† Email address for correspondence: alice@maths.leeds.ac.uk

‡ As pointed out by Moffatt (1978), terms involving time derivatives may also appear; however, these may be expressed in terms of spatial derivatives by back substitution.

where C is the sum of its mean and fluctuating components, $C = \overline{C} + c$. The tensors D_{ij} (the diffusion tensor) and E_{ijk}, which depend on the statistics of the velocity field, may be regarded as transport coefficients for the mean field $\overline{C}$. Similarly, the e.m.f. in MHD turbulence may be expressed as

$$\mathscr{E}_i \equiv \left(\overline{\boldsymbol{u} \times \boldsymbol{b}}\right)_i = \alpha_{ij} \overline{B}_j + \beta_{ijk} \frac{\partial \overline{B}_j}{\partial x_k} + \cdots, \tag{1.2}$$

where the magnetic field $\boldsymbol{B}$ has been decomposed as $\boldsymbol{B} = \overline{\boldsymbol{B}} + \boldsymbol{b}$. The pseudo-tensors α_{ij}, which encompasses the α-effect of mean field electrodynamics, and β_{ijk}, the magnetic diffusion tensor, may again be regarded as transport coefficients. In the most general formulation the transport tensors may be functions of the large spatial scale. Of these two problems, the turbulent transport of vector quantities is the more complex and difficult to understand, with extra effects arising from the stretching and reorientation of the vector field; for example, in the MHD problem there is the possibility of magnetic field amplification through the α-effect. Thus, a promising approach to enhancing our understanding of the vector problem is to compare and contrast the transport of vectors and scalars for the same turbulent flow. Moreover, by considering flows with advantageous symmetry properties, the scalar transport problem simply becomes part of the broader vector problem. This approach, which has been used successfully in a related study of cat's-eye flows by Childress & Soward (1989), allows the calculation of α_{ij} and D_{ij}. In this paper we shall be concerned only with the kinematic evolution; the scalar C and magnetic field $\boldsymbol{B}$ are assumed to be passive, transported by a prescribed velocity field $\boldsymbol{u}(\boldsymbol{x}, t)$.

Specifically, we consider flows of the form $\boldsymbol{u}(x, y, t)$, invariant to translations in the z-direction. Such flows possess three beneficial characteristics. First, as noted above and discussed in detail in § 2, they allow the study of the vector and scalar problems purely within the framework of the vector problem. Second, they allow us to incorporate a large range of scales in our numerical simulations of the flow. Third, for magnetic fields that are also independent of z, the fluctuating magnetic field $\boldsymbol{b}$ is sustained only in the presence of a mean field $\overline{\boldsymbol{B}}$, thereby allowing an unambiguous interpretation of expression (1.2); for more general flows the fluctuating magnetic field can be self-sustaining (a small-scale dynamo) and problems can then arise with both the measurement and interpretation of $\boldsymbol{\alpha}$, as noted by Cattaneo & Hughes (2009).

Simple steady cellular flows that take the form $\boldsymbol{u}(x, y)$ and possess just one spatial scale have been utilized in studies of transport coefficients over many years; these date back to the pioneering work of Roberts (1970), with subsequent modifications by, for example, Plunian & Rädler (2002), Childress & Soward (1989) and Courvoisier, Gilbert & Ponty (2005). The natural extension to time-periodic flows of the form $\boldsymbol{u}(x, y, t)$ has been considered by, for example, Majda & Kramer (1999) for scalar diffusion and by Courvoisier, Hughes & Tobias (2006) and Rädler & Brandenburg (2009) for the α-effect. A common feature of all these studies is that the flows considered are spatially periodic; spatial averages therefore are, necessarily, taken over identical cells acting in concert. The advantage of using such an approach is that the resulting averages are well defined, leading to unambiguous determination of the transport coefficients. The drawback is that the averages may not be indicative of those emerging from truly turbulent flows, characterized by a range of decorrelated spatial and temporal scales.

In fully developed turbulence it is difficult to disentangle, let alone quantify, the influence on the transport coefficients of spatial and temporal decorrelations in the flow. This can be seen, for example, in the determination of the mean e.m.f. in simulations of rotating convective turbulence (Cattaneo & Hughes 2006; Hughes & Cattaneo 2008), which, furthermore, highlights the difficulties in obtaining a meaningful average of the e.m.f.. In order to elucidate the distinct roles of spatial and temporal decorrelations, one approach is to build upon the results obtained from synchronized (i.e. steady or time-periodic) flows by incorporating separately, and in a controlled manner, temporal and spatial decoherence. The former problem has been studied by Courvoisier *et al.* (2006) and Courvoisier (2008), who demonstrated that increasing temporal decoherence leads to a reduction in the magnitude and Rm-dependence of the α-effect. Here we address the complementary question of the influence on the transport coefficients of spatial decorrelation. We consider time-periodic cellular flows, periodic in space over large domains encompassing many cells, and introduce spatial decorrelation in a quantifiable fashion so as to study its impact on the nature of the transport for both scalars and vectors. Averages are taken over the periodic domains and over the time periodicity of the flows; clearly, in this case, the coefficients of the transport tensors are constants.

In § 2 we first outline the general formulation of mean field theory, for the transport of both scalar and magnetic fields. We then discuss the specific case of two-dimensional flows and show how, in this case, the scalar transport problem simply becomes part of the magnetic problem. In § 3 we discuss the specific flows used, their properties and the manner in which spatial decoherence is introduced. Section 4 contains the results of the determination of the transport coefficients, and § 5 a discussion of their implications.

2. Mean field theory

2.1. *The general formulation*

The evolution of a magnetic field $\boldsymbol{B}$, embedded in an electrically conducting fluid moving with velocity $\boldsymbol{u}$ and with uniform magnetic diffusivity, is described, in dimensionless form, by the induction equation

$$\frac{\partial \boldsymbol{B}}{\partial t} = \nabla \times (\boldsymbol{u} \times \boldsymbol{B}) + \frac{1}{Rm}\nabla^2 \boldsymbol{B}, \tag{2.1}$$

where the magnetic Reynolds number Rm denotes the ratio of advection of the magnetic field to its diffusion. In addition, the magnetic field must satisfy the solenoidal constraint

$$\nabla \cdot \boldsymbol{B} = 0. \tag{2.2}$$

Equation (2.1) describes the transport of a vector field; the corresponding equation for a passive scalar field C is given by

$$\frac{\partial C}{\partial t} + \boldsymbol{u} \cdot \nabla C = \frac{1}{Rm}\nabla^2 C. \tag{2.3}$$

Here Rm^{-1} denotes the dimensionless diffusivity of C; we have chosen to use the same symbol as in (2.1) since we shall be making direct comparisons between the vector and scalar problems. The regime of interest for both cases is that of large Rm. The magnetic problem is motivated by astrophysical considerations, for which Rm is typically huge; similarly, the mixing of scalars is often considered for high Péclet number, which is equivalent to high Rm in (2.3).

For both cases we shall be addressing the dynamics of large-scale quantities, traditionally studied within the framework of mean field theory (see, for example, Roberts 1994). The starting point is to decompose the magnetic and scalar fields into the sum of average and fluctuating components, i.e.

$$\boldsymbol{B} = \overline{\boldsymbol{B}} + \boldsymbol{b}, \qquad C = \overline{C} + c, \tag{2.4}$$

where an overbar denotes a suitable averaging operation. Substitution into (2.1) and (2.3), and making the simplifying assumption that there is no mean flow, then leads to the following evolution equations for the mean magnetic and scalar fields:

$$\frac{\partial \overline{\boldsymbol{B}}}{\partial t} = \nabla \times (\overline{\boldsymbol{u} \times \boldsymbol{b}}) + \frac{1}{Rm}\nabla^2 \overline{\boldsymbol{B}}, \tag{2.5}$$

$$\frac{\partial \overline{C}}{\partial t} = -\nabla \cdot \overline{c\boldsymbol{u}} + \frac{1}{Rm}\nabla^2 \overline{C}. \tag{2.6}$$

To close these equations, it is necessary to express the fluxes $\overline{\boldsymbol{u} \times \boldsymbol{b}}$ and $\overline{c\boldsymbol{u}}$ in terms of the mean magnetic and scalar fields. The linearity in $\boldsymbol{B}$ and C of (2.1) and (2.3) suggests the following expansions in terms of the mean fields and their derivatives (see, for example, Moffatt 1983), where higher order derivatives have been neglected:

$$\overline{\boldsymbol{u} \times \boldsymbol{b}} = \boldsymbol{\alpha} \cdot \overline{\boldsymbol{B}} + \boldsymbol{\beta} \cdot \nabla \overline{\boldsymbol{B}}, \tag{2.7}$$

$$\overline{c\boldsymbol{u}} = -\boldsymbol{D} \cdot \nabla \overline{C}, \tag{2.8}$$

where $\boldsymbol{\alpha}$ and $\boldsymbol{\beta}$ are pseudo-tensors and $\boldsymbol{D}$ is a tensor. The level of truncation in (2.7) and (2.8) is determined by consistency with the full equations (2.1) and (2.3), which possess spatial derivatives up to second order; for the case considered here, in which the entries in $\boldsymbol{\alpha}$, $\boldsymbol{\beta}$ and $\boldsymbol{D}$ are constants, the inclusion of further terms in (2.7) and (2.8) would lead to terms in (2.5) and (2.6) with spatial derivatives only of higher order.

Formal substitution of the expression for the mean e.m.f. from (2.7) into (2.5) leads to the mean magnetic induction equation

$$\frac{\partial \overline{\boldsymbol{B}}}{\partial t} = \nabla \times (\boldsymbol{\alpha} \cdot \overline{\boldsymbol{B}}) + \nabla \times (\boldsymbol{\beta} \cdot \nabla \overline{\boldsymbol{B}}) + \frac{1}{Rm}\nabla^2 \overline{\boldsymbol{B}}. \tag{2.9}$$

The $\boldsymbol{\alpha}$ tensor encompasses two distinct physical effects. Its symmetric part acts to regenerate poloidal (toroidal) magnetic field from toroidal (poloidal) field; this is the famous 'α-effect' of mean field electrodynamics, which lies at the heart of much astrophysical dynamo modelling. It relies on a lack of reflectional symmetry in the motion, the simplest measure of which is the flow helicity. The antisymmetric part of $\boldsymbol{\alpha}$ gives rise to a mean transport velocity, often described as 'magnetic pumping' or 'turbulent diamagnetism'. For the simplest case of isotropic turbulence, $\boldsymbol{\beta}$ must take the form $\beta_{ijk} = \beta \epsilon_{ijk}$; it is then easily seen from (2.9) that β can be interpreted as a turbulent magnetic diffusivity. More generally though, the physical interpretation of $\boldsymbol{\beta}$ is not so straightforward. The nature of the $\boldsymbol{\alpha}$ and $\boldsymbol{\beta}$ tensors is discussed in detail in Moffatt (1978) and Krause & Rädler (1980).

For the case of a scalar field, substitution from (2.8) into (2.6) leads to the following evolution equation for the mean field:

$$\frac{\partial \overline{C}}{\partial t} = \nabla \cdot (\boldsymbol{D} \cdot \nabla \overline{C}) + \frac{1}{Rm}\nabla^2 \overline{C} \tag{2.10}$$

$$= \nabla \cdot (\boldsymbol{D}^E \cdot \nabla \overline{C}), \tag{2.11}$$

where

$$D_{ij}^{E} = \frac{1}{Rm}\delta_{ij} + \frac{1}{2}(D_{ij} + D_{ji}) \tag{2.12}$$

is a symmetric effective diffusivity tensor. Note that whereas (2.10) is true in general, expression (2.11) has made use of the spatial independence of $\boldsymbol{D}$ pertinent to the case studied in this paper; in general, when $\boldsymbol{D}$ is spatially dependent, then its antisymmetric term is also of significance, representing an effective transport velocity for $\overline{C}$ (see Moffatt 1983; Cattaneo, Hughes & Proctor 1988).

Describing the evolution of the mean magnetic field $\boldsymbol{B}$ or mean scalar field $\overline{C}$ therefore relies on evaluating, or at least approximating, the tensors $\boldsymbol{\alpha}$, $\boldsymbol{\beta}$ and $\boldsymbol{D}$. This involves the determination of the fluctuating fields ($\boldsymbol{b}$ or c), which, in general, presents a problem of equal difficulty to that of solving the unaveraged equations (2.1) or (2.3). Progress can be made either via some kind of closure scheme (e.g. the EDQNM scheme developed for MHD by Pouquet, Frisch & Léorat 1976) or by considering certain limiting cases for which the equations for the fluctuating fields simplify and can be solved rigorously. For example, for three-dimensional turbulence with a short correlation time τ (and assuming isotropy for simplicity, with $\alpha_{ij} = \alpha\delta_{ij}$, $\beta_{ijk} = \beta\epsilon_{ijk}$ and $D_{ij} = D\delta_{ij}$) it can be shown that (Taylor 1921; Krause & Rädler 1980)

$$\alpha = -\frac{\tau}{3}\overline{\boldsymbol{u}\cdot\nabla\times\boldsymbol{u}}, \quad \beta = D = \frac{\tau}{3}\overline{\boldsymbol{u}^2}. \tag{2.13}$$

Thus, in this case, the transport coefficients depend on just the correlation time τ (assumed small) and on global properties of the flow; in particular, the helicity for α and the kinetic energy for β and D. One of our objectives is to examine whether, more generally, expressions such as (2.13) can be valid. It should be noted that, in general, the diffusion of a passive scalar is distinct from that of a passive vector for three-dimensional turbulence, even for the simplest case of stationarity, homogeneity and isotropy (Kraichnan 1976; Knobloch 1977; Moffatt 1978). This difference persists in two-dimensional turbulence if the transport coefficients are space dependent, as shown by Cattaneo *et al.* (1988). A detailed study of the relation between $\boldsymbol{D}$ and $\boldsymbol{\beta}$ is beyond the scope of this paper. Here we are interested in comparing the scalar and vector problems in order to determine whether a mean field treatment is similarly valid in both cases. Thus we shall consider the nature of $\boldsymbol{\alpha}$ and $\boldsymbol{D}$ for a range of flows that have comparable energies and helicities, but which vary in the extent of their spatial correlation.

2.2. *Two-dimensional flows*

As noted in §1, for three reasons it is helpful to consider two-dimensional flows; assuming also incompressibility, the velocity can be expressed as

$$\boldsymbol{u}(x, y, t) = (\partial_y\psi(x, y, t), -\partial_x\psi(x, y, t), w(x, y, t)). \tag{2.14}$$

Furthermore, we shall restrict attention to flows for which

$$w = r\psi, \quad (r \text{ constant}) \tag{2.15}$$

although this restriction is not important in the exposition that follows. For convenience, we will refer to the xy-plane as the horizontal plane and to the z-direction as the vertical, although gravity plays no part in the present study.

The $\boldsymbol{\alpha}$ tensor is determined via solution of the induction equation for the fluctuating magnetic field $\boldsymbol{b}$, in the presence of a uniform imposed mean field $\boldsymbol{B}_0$. This takes the

$\boldsymbol{B}_0$	$\boldsymbol{D}^E$	$\boldsymbol{\alpha}$
$B_0\,\boldsymbol{e}_x$	$D^E_{22} = Rm^{-1}\left(\overline{b_H^2}/B_0^2 + 1\right)$	$\alpha_{11} = \mathscr{E}_x B_0^{-1}$ and $\alpha_{21} = \mathscr{E}_y B_0^{-1}$
$B_0\,\boldsymbol{e}_y$	$D^E_{11} = Rm^{-1}\left(\overline{b_H^2}/B_0^2 + 1\right)$	$\alpha_{21} = \mathscr{E}_x B_0^{-1}$ and $\alpha_{22} = \mathscr{E}_y B_0^{-1}$

TABLE 1. Components of the tensors $\boldsymbol{D}^E$ and $\boldsymbol{\alpha}$ that can be determined by imposing an x- or y-directed mean field.

form

$$(\partial_t - Rm^{-1}\nabla^2)\boldsymbol{b} + \boldsymbol{u}\cdot\nabla\boldsymbol{b} = (\boldsymbol{B}_0 + \boldsymbol{b})\cdot\nabla\boldsymbol{u}. \tag{2.16}$$

We seek magnetic field solutions that are independent of z. This choice has two advantages. First, (2.16) is dependent on only two spatial dimensions and can therefore be solved efficiently, by numerical techniques, for high values of Rm and for large computational domains. Second, small-scale dynamo action is not possible in this case (Cowling 1933); thus, in the absence of an imposed mean field, the magnetic field $\boldsymbol{b}$ will decay. This ensures that $\boldsymbol{\alpha}$ is linearly and homogeneously related to the mean field, as assumed by (2.7).

Since the magnetic field is solenoidal we may express $\boldsymbol{b}(x, y, t)$ in the form

$$\boldsymbol{b}(x, y, t) = \nabla \times (a(x, y, t)\boldsymbol{e}_z) + b_z(x, y, t)\boldsymbol{e}_z, \tag{2.17}$$

where $\boldsymbol{e}_z$ is the unit vector in the z-direction. Substituting expression (2.17) into (2.16) then leads to the following evolution equations for a and b_z:

$$(\partial_t - Rm^{-1}\nabla^2)a + \boldsymbol{u}_H\cdot\nabla a = \boldsymbol{B}_0\cdot\nabla\psi, \tag{2.18}$$

$$(\partial_t - Rm^{-1}\nabla^2)b_z + \boldsymbol{u}_H\cdot\nabla b_z = \boldsymbol{B}_0\cdot\nabla w + \boldsymbol{b}\cdot\nabla w, = r\,\boldsymbol{B}_0\cdot\nabla\psi - r\,\boldsymbol{u}_H\cdot\nabla a, \tag{2.19}$$

using (2.15), where $\boldsymbol{u}_H$ denotes the horizontal velocity field.

Thus, for flows of the form (2.14) the evolution equation for a corresponds to that for a passive scalar field in the presence of a uniform imposed mean gradient $(\partial_x\overline{A}, \partial_y\overline{A}) = (-B_{0y}, B_{0x})$ (Childress & Soward 1989). We can therefore use the evolution of a to determine the effective diffusivity $\boldsymbol{D}^E$. Indeed, using the theorem of Zel'dovich (1957) (see the Appendix for the algebra), it can be shown that

$$D_{ij}\,\partial_i\overline{A}\,\partial_j\overline{A} = Rm^{-1}\overline{b_H^2}. \tag{2.20}$$

Therefore, the components of $\boldsymbol{D}$ can be determined simply by measuring the magnetic energy in the horizontal field; $\boldsymbol{D}^E$ follows from (2.12).

For flows that are independent of z, the α-effect and the turbulent diffusion are highly anisotropic and act solely in the xy-plane. We therefore concentrate on the 2×2 parts of $\boldsymbol{\alpha}$ and $\boldsymbol{D}^E$ that relate horizontal quantities. The components of the $\boldsymbol{\alpha}$ tensor are determined in the usual way by calculating the mean electromotive force $\boldsymbol{\mathscr{E}} = \overline{\boldsymbol{u}\times\boldsymbol{b}}$. For a uniform mean field, (2.7) implies that $\boldsymbol{\mathscr{E}} = \boldsymbol{\alpha}\cdot\boldsymbol{B}_0$. We can thus obtain all four components of $\boldsymbol{\alpha}$ by taking $\boldsymbol{B}_0$ to be successively in the x- and y-directions. A summary of the quantities that can be determined with the present setup is given in table 1.

Equations (2.18) and (2.19) are solved using a two-dimensional pseudo-spectral discretization in space and a second-order Runge–Kutta time-stepping scheme. The code is optimized to run on machines with parallel architecture. The initial conditions $a = b_z = 0$ ensure that there is no mean field other than the imposed $\boldsymbol{B}_0$.

3. The flows and their properties

In this investigation we consider velocity fields of the form (2.14). The specific flows we use are developed from well-known cellular flows, namely the circularly polarised (CP) flow of Galloway & Proctor (1992) and the modulated waves (MW+) flow of Otani (1993), for which the stream functions ψ are given by ψ^{CP} and ψ^{MW} respectively, where

$$\psi^{CP}(x, y, t) = \sqrt{3/2}(\cos(x + \epsilon\cos\omega t) + \sin(y + \epsilon\sin\omega t)), \tag{3.1}$$

$$\psi^{MW}(x, y, t) = 2\cos^2 t\cos x - 2\sin^2 t\cos y. \tag{3.2}$$

The z-components of both flows are given by $w = -\psi$, which corresponds to setting $r = -1$ in (2.15) and which ensures that the motions are maximally helical, here with a negative helicity. The determination of the α-effect in these flows has formed the subject of previous investigations, which show that both flows have a strong, albeit highly Rm-dependent α-effect (Courvoisier 2008). Both of these velocity fields also display regions of Lagrangian chaos; this makes them efficient small-scale dynamos (Childress & Gilbert 1995), which was the original focus for their study. Although we shall not be concerned here with small-scale dynamo action, the transport properties that we are investigating are also related to the chaotic properties of the flows (see, for example, the books by Ottino 1989 and Sturman, Ottino & Wiggins 2006).

Flows such as (3.1) and (3.2) do however possess a number of characteristics that are not typical of turbulent flows. In particular, they are 2π-periodic in space and time and therefore have infinite spatial and temporal Eulerian correlations. Turbulence is characterized by a finite correlation time and by spatial decorrelations between turbulent eddies. In an earlier paper we described the influence on the e.m.f. of introducing temporal decorrelation into the CP flow (Courvoisier *et al.* 2006) – this was achieved by incorporating a random phase into the temporal dependence of the flow. As noted above, that study, which was concerned solely with the determination of the α-effect, demonstrated that the magnitude of α decreases and that its Rm-dependence weakens as the correlation time of the flow is reduced.

In the present paper, we are interested in the role of *spatial* decorrelations on the transport coefficients of the flow; we therefore systematically modify the forms of the velocity fields from those given in (3.1) and (3.2) so as to introduce these. The velocities (3.1) and (3.2) form a periodic array of cells with a single well-defined length scale, corresponding to the size of the computational domain. This can easily be generalized to the case where the length scale of the flow is smaller than that of the system size. We therefore reduce the scale of the motions to $2\pi/k$, where k is an integer greater than 2. At this point the velocity takes the form of a $k \times k$ array of cells in a 2π-periodic domain, all correlated in space and acting in concert in time. The next step is to introduce phase shifts between neighbouring cells in the array, which breaks the spatial periodicity of the motions on the smaller (i.e. $2\pi/k$) scale. The degree of spatial decorrelation can then be controlled by the properties of the distribution from which the random phases are selected.

Mathematically this procedure corresponds to selecting velocity fields of the form

$$\boldsymbol{u}_k(x, y, t) = (\partial_y\psi_k(x, y, t), -\partial_x\psi_k(x, y, t), r_k\psi_k(x, y, t)), \tag{3.3}$$

where ψ_k is $2\pi/k$-periodic in space and time. We consider two different families of stream functions, namely

$$\psi_k^{CP}(x, y, t) = \sum_{i,j=1}^{k} A_k(\cos(kx + \epsilon_k\cos(\omega_k t + \phi_{ij})) + \sin(ky + \epsilon_k\sin(\omega_k t + \phi_{ij})))\, h_{ij}(kx, ky) \tag{3.4}$$

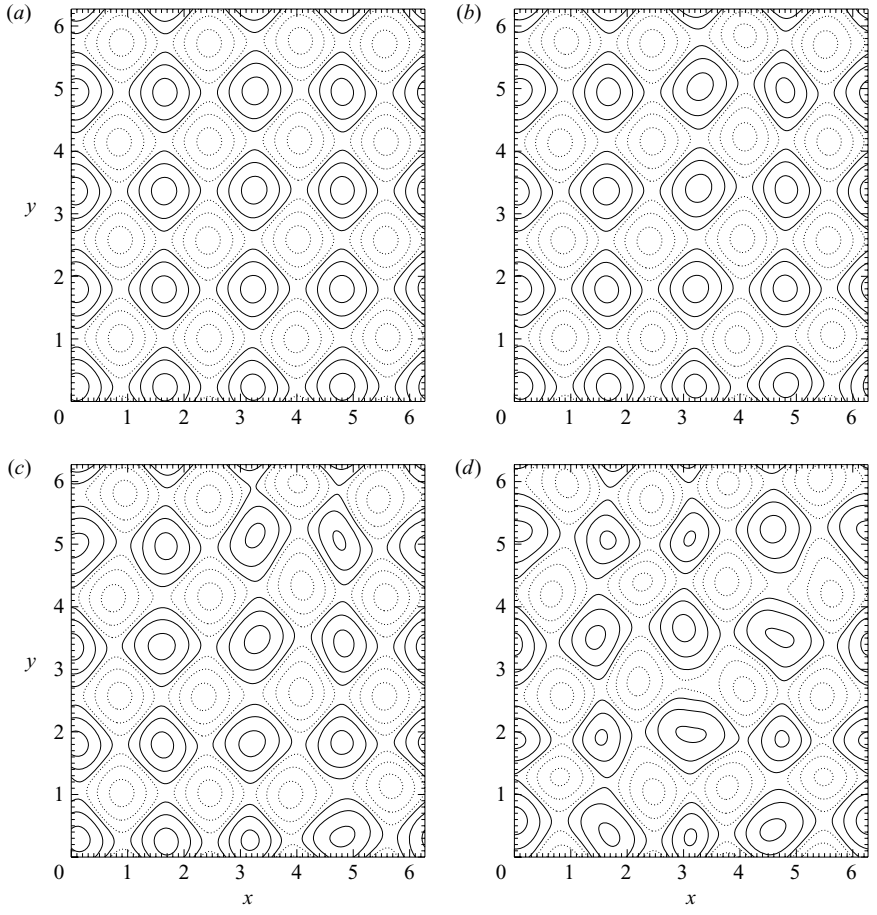

FIGURE 1. Snapshots of the streamlines for flow (3.4) with different phase distributions and $k=4$. (*a*) $\boldsymbol{\phi} \in \mathcal{N}(0, 0.2)$, (*b*) $\boldsymbol{\phi} \in \mathcal{N}(0, 0.5)$, (*c*) $\boldsymbol{\phi} \in \mathcal{N}(0, 1)$ and (*d*) $\boldsymbol{\phi} \in \mathcal{U}([0, 2\pi])$. The dotted lines correspond to negative values of the stream function.

and

$$\psi_k^{MW}(x, y, t) = \sum_{i,j=1}^{k} A_k(2\cos(kx)\cos^2(\omega_k t + \phi_{ij}) - 2\cos(ky)\sin^2(\omega_k t + \phi_{ij}))\, h_{ij}(kx, ky). \quad (3.5)$$

We shall discuss below the precise forms adopted for h_{ij} and ϕ_{ij}. However, the general nature of the flows is probably best appreciated by inspection of figures 1 and 2, which show snapshots of the streamlines.

The functions h_{ij} are masking functions that are non-zero on a square of side $4\pi/k$ centred on $(x, y) = ((2i-1)\pi/k, (2j-1)\pi/k)$ and are zero elsewhere. Specifically we set

$$\begin{aligned} h_{ij}(x, y) &= (\tanh((-1)^{i+1}\sin(x/2))/\tanh 1 + 1)(\tanh((-1)^{j+1}\sin(y/2))/\tanh 1 + 1)/4 \\ &\quad \text{for } (x, y) \in [(2i-3)\pi, (2i+1)\pi] \times [(2j-3)\pi, (2j+1)\pi] \\ &= 0 \quad \text{otherwise.} \end{aligned}$$

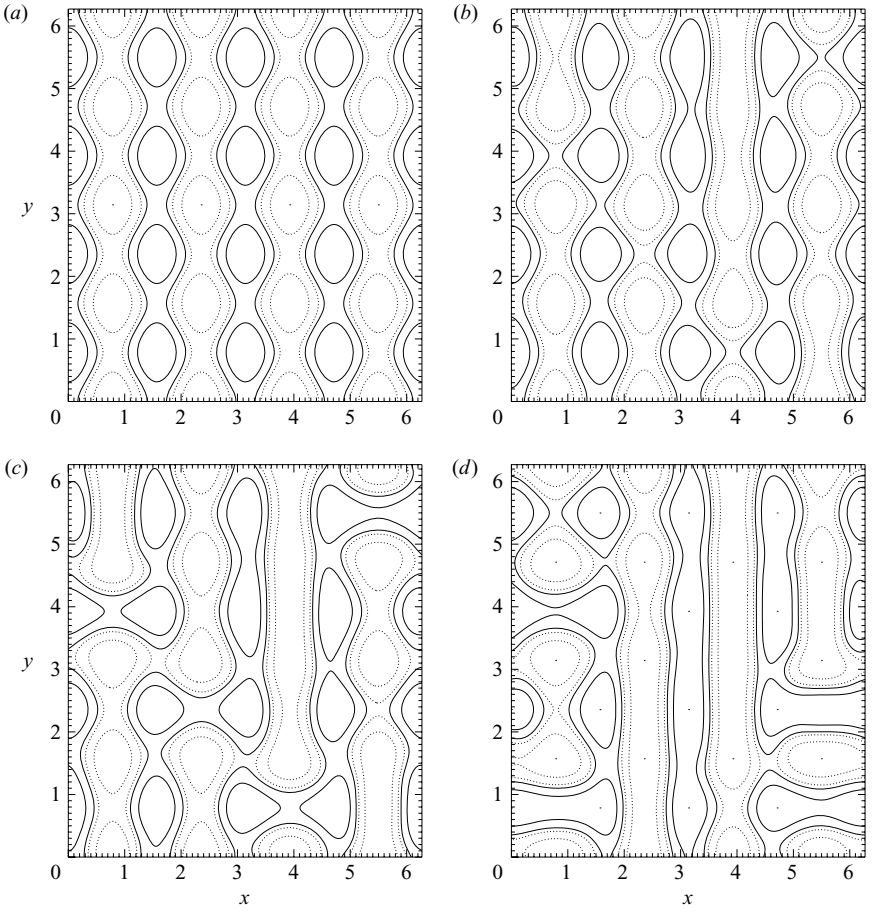

FIGURE 2. Snapshots of the streamlines for flow (3.5) with different phase distributions and $k=4$. (*a*) $\boldsymbol{\phi}=\mathbf{0}$, (*b*) $\boldsymbol{\phi}\in\mathcal{N}(0, 0.2)$, (*c*) $\boldsymbol{\phi}\in\mathcal{N}(0, 0.5)$ and (*d*) $\boldsymbol{\phi}\in\mathcal{U}([0, 2\pi])$. The dotted lines correspond to negative values of the stream function.

The spatial decorrelations between neighbouring cells are introduced via the phases ϕ_{ij}. For each cell in the $k\times k$ array, ϕ_{ij} is drawn from a specified distribution. In particular we consider either a uniform distribution on $[0, 2\pi]$ (i.e. $\boldsymbol{\phi}\in\mathcal{U}([0, 2\pi])$) or, more usually, a normal distribution with mean zero and variance λ^2 (i.e. $\boldsymbol{\phi}\in\mathcal{N}(0, \lambda)$). Clearly the degree of decorrelation in the flow can then be controlled by the standard deviation λ of the distribution; as $\lambda\to 0$ all the phases are identical and the cells return to perfect correlation, whilst as λ increases so does the spatial decorrelation in the flow.

The motions (3.4) and (3.5) therefore consist of a 2π-periodic pattern formed by an array of k^2 cells with different phase shifts ϕ_{ij}, which introduce spatial decorrelations in the x- and y-directions. The complicated functions h_{ij} serve only to ensure that the transition between neighbouring cells is smooth.

In order to make comparisons between flows with different spatial scales, it is necessary to adopt scalings for the coefficients A_k, ϵ_k, ω_k and r_k. Recall that for $k=1$, the scale of the flow is that of the computational domain; here $\psi_1^{CP}=\psi^{CP}$ and $\psi_1^{MW}=\psi^{MW}$. However for $k>1$ and $\boldsymbol{\phi}=0$ (i.e. no spatial decorrelation), motions

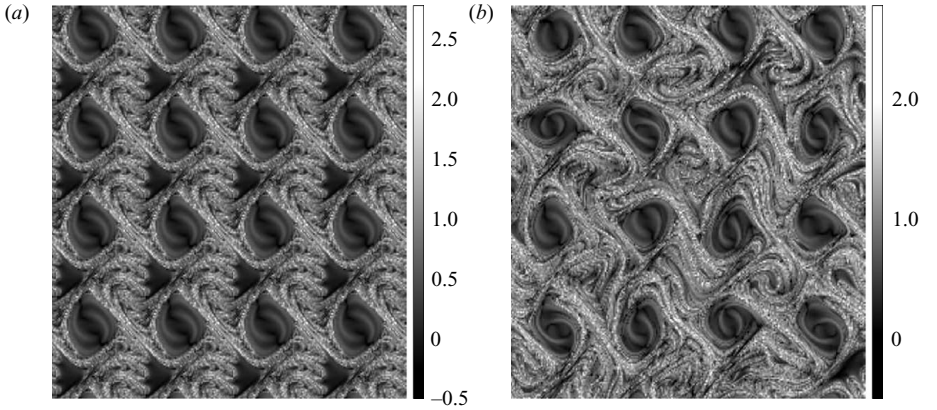

FIGURE 3. Finite-time ($t = 20$) Lyapunov exponents for the CP flow with (a) $\boldsymbol{\phi} = \mathbf{0}$ and (b) $\boldsymbol{\phi} \in \mathscr{U}([0, 2\pi])$.

(3.4) and (3.5) have a spatial periodicity of $2\pi/k$, and the corresponding turnover times and local values of Rm are altered. To ensure that the results obtained for $k > 1$ can be meaningfully compared with the existing results for $k = 1$, we need to rescale the k-dependent quantities appropriately. Following Cattaneo & Tobias (2005), which contains a detailed description of the rationale for the scalings, we take

$$A_k = A_1/k, \quad \epsilon_k = \epsilon_1, \quad \omega_k = k\omega_1 \quad \text{and} \quad r_k = kr_1. \tag{3.6}$$

For flow (3.4) we set $A_1 = \sqrt{3/2}$ and $\epsilon_1 = 0.75$, whilst for flow (3.5) we set $A_1 = 1$; for both flows we choose $\omega_1 = 1$, $r_1 = -1$. The scaling of A_k ensures that the kinetic energy averaged over space and time is independent of k. The relevant magnetic Reynolds number is based on the scale of the cell (i.e. $2\pi/k$); this is defined as $Rm_k = Rm/k$, where Rm is the magnetic Reynolds number based on the total system size.

For $k > 1$ and $\boldsymbol{\phi} \neq 0$, the regime of interest here, spatial decorrelations are introduced and the flows are no longer periodic on the scale $2\pi/k$. To illustrate the consequences of this, figures 1 and 2 present snapshots of the streamlines of flows (3.4) and (3.5), respectively, for ϕ_{ij} drawn from phase distributions of increasing randomness. These figures demonstrate how the cells become distorted in the CP flow and how the channels present in the MW+ flow are affected by the decorrelations and may even disappear.

Clearly the decorrelation of neighbouring cells has a significant impact on the Eulerian properties of the flow. However, it is often the Lagrangian properties of a flow that are significant in determining the transport coefficients. As noted above, both the CP and the MW+ flows are characterized by large regions of Lagrangian chaos, which are believed to be important for transport and mixing. It is therefore of interest to determine how introducing spatial decorrelations into the flows modifies the Lagrangian chaos. Figures 3 and 4 show density plots of the finite-time Lyapunov exponents for flows (3.4) and (3.5) respectively. These are calculated for $k = 4$ with $\boldsymbol{\phi} = \mathbf{0}$ and $\boldsymbol{\phi} \in \mathscr{U}([0, 2\pi])$. The chaotic regions increase in size for a random phase distribution, but substantial integrable islands remain, especially in the case of the decorrelated CP flow (3.4).

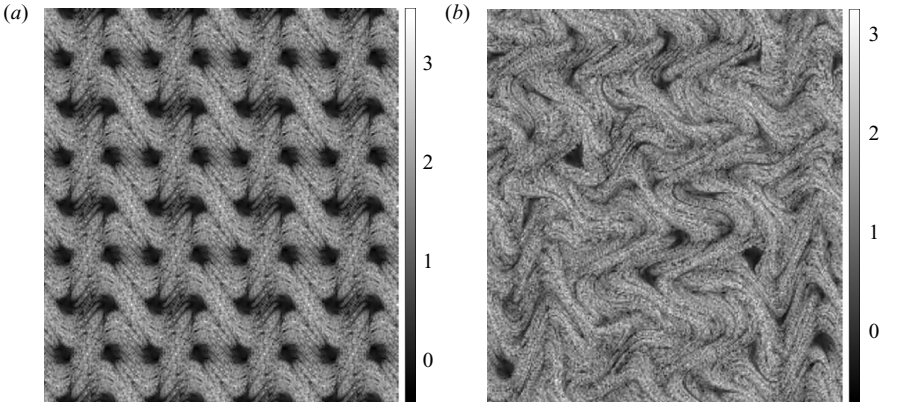

FIGURE 4. Finite-time ($t = 20$) Lyapunov exponents for the MW+ flow with (a) $\boldsymbol{\phi} = \mathbf{0}$ and (b) $\boldsymbol{\phi} \in \mathscr{U}([0, 2\pi])$.

As noted in § 1, the notion of averaging is of vital importance in determining the transport properties of the flows. For the flows described by (3.4) and (3.5), which are 2π-periodic in both space and time, it is convenient to define a spatio-temporal average by

$$\overline{C} = \frac{1}{8\pi^3} \int_0^{2\pi} \int_0^{2\pi} \int_0^{2\pi} C(x, y, t)\, \mathrm{d}x\, \mathrm{d}y\, \mathrm{d}t. \tag{3.7}$$

Owing to the periodicity of the flows and of the resulting magnetic field, it should be noted that all averages considered in this paper are well defined.

Once an unambiguous averaging procedure has been identified it is possible to calculate mean properties of the flows. Relations (3.6) imply that, in the absence of phase perturbations (i.e. when $\boldsymbol{\phi} = \mathbf{0}$),

$$\overline{u_k^2} = \overline{u_1^2} = 3, \quad \overline{\boldsymbol{u}_k \cdot \nabla \times \boldsymbol{u}_k} = k\overline{\boldsymbol{u}_1 \cdot \nabla \times \boldsymbol{u}_1} = -3k. \tag{3.8}$$

Hence, for this case, the flows are maximally helical, with a negative helicity. For all the phase distributions and values of k chosen in this study, the kinetic energy and the helicity of the decorrelated flows remain within 15 % of their values for $\boldsymbol{\phi} = \mathbf{0}$. The motions are thus still substantially helical and are therefore, at least naïvely, prime candidates for a strong α-effect.

For $\boldsymbol{\phi} = \mathbf{0}$, the rescaling given by (3.6) also implies that $\boldsymbol{\alpha}$ and $\boldsymbol{D}^E$ are independent of k; the cases with no decorrelation can thus be used as a benchmark for any value of k, allowing meaningful comparisons between different choices of k. Furthermore, in this correlated case, flows (3.4) and (3.5) have the symmetry properties of the CP and MW+ flows respectively. They are invariant under a rotation of $\pi/2$ with respect to the z-axis, together with appropriate shifts in space and time. This implies (see, for example, Courvoisier 2008) that, for no decorrelation,

$$\alpha_{11} = \alpha_{22} = \alpha, \qquad \alpha_{12} = -\alpha_{21} = -\gamma, \tag{3.9}$$

$$D^E_{11} = D^E_{22} = D^E, \quad D^E_{12} = D^E_{21} = 0. \tag{3.10}$$

For the flow (3.5), an additional symmetry yields $\gamma = 0$.

When the elements of $\boldsymbol{\phi}$ are chosen randomly, the x- and y-directions are no longer equivalent and relations (3.9) and (3.10) are not expected to hold in general. However, for sufficiently large arrays of cells one expects the symmetry to be restored

Rm_k	4	16	64	128	256	1024
$k=1$	32^2	32^2	64^2	64^2	128^2	256^2
$k=4$	128^2	128^2	256^2	–	512^2	1024^2
$k=16$	512^2	512^2	1024^2	1024^2	2048^2	–

TABLE 2. Spatial resolution used for the values of k and Rm investigated.

on average, although it is not clear *a priori* how many cells may be needed for this to be achieved.

4. Determination of the transport coefficients

We solve (2.18) and (2.19) with a uniform mean field imposed in the x-direction to determine α_{11} and D^E_{22}, and in the y-direction to determine α_{22} and D^E_{11}. The values of k and Rm investigated are given in table 2, together with the spatial resolution used. All the results in this paper are given in terms of the small-scale magnetic Reynolds number Rm_k.

To illustrate the changes in the induced magnetic field as the spatial correlations are reduced, we present snapshots of b_x for different phase distributions in figures 5 (for flow (3.4)) and 6 (for flow (3.5)). We observe that as the velocity fields become more spatially random, there are fewer regions of strong magnetic fields. It seems that even though the field strength can be increased locally, flux cancellation dominates on average.

In the following subsections, we describe successively the behaviour of the α-effect and that of turbulent diffusion.

4.1. *The α-effect*

In the present study we are concerned specifically with the α-effect so, from (3.9), we need only to consider the diagonal entries to the $\boldsymbol{\alpha}$ tensor. We begin by describing how the α-effect varies as the spatial correlations in the flows are reduced. To this end, we take the components of $\boldsymbol{\phi}$ from a normal distribution and increase the standard deviation λ from 0 to 1, whilst keeping the magnetic Reynolds number constant at $Rm_k = 128$ and $k = 16$. The dependence on λ of α_{11} and α_{22}, normalized by the r.m.s. velocity, is shown in figure 7. For both flows, α_{11} and α_{22} vary smoothly and monotonically as the motions become more random.

For flow (3.4), α_{11} decreases monotonically and gets close to zero. At $\lambda = 1$, α_{11}/u_{rms} has decreased to just 7 % of its value for $\lambda = 0$. For a uniform distribution, $\alpha_{11}/u_{rms} = 0.016 \pm 0.032$, with a spread calculated over four realizations of the random phases. The other diagonal component, α_{22}, remains close to α_{11} until $\lambda \approx 0.5$. For more strongly decorrelated flows, α_{11} and α_{22} are distinct and as α_{11} decreases towards zero, α_{22} changes sign and reaches a positive value with a normalized magnitude for $\lambda = 1$ equal to 15 % of that at $\lambda = 0$. Further calculations performed for $k = 4$ show that α_{22} starts to differ from α_{11} for even lower values of λ. We anticipate that the symmetry between the two diagonal components of $\boldsymbol{\alpha}$ will be restored on average as k is increased, but this question remains open to further investigations.

For flow (3.5), α_{11} and α_{22} coincide and rapidly decrease in magnitude, even for low values of λ. It seems that they reach a limit of $\alpha_{11}/u_{rms} = \alpha_{22}/u_{rms} \approx 0.34$, which also equals α_{11}/u_{rms} with $\boldsymbol{\phi} \in \mathscr{U}([0, 2\pi])$ and is less than a third of their value for the unperturbed case $\lambda = 0$.

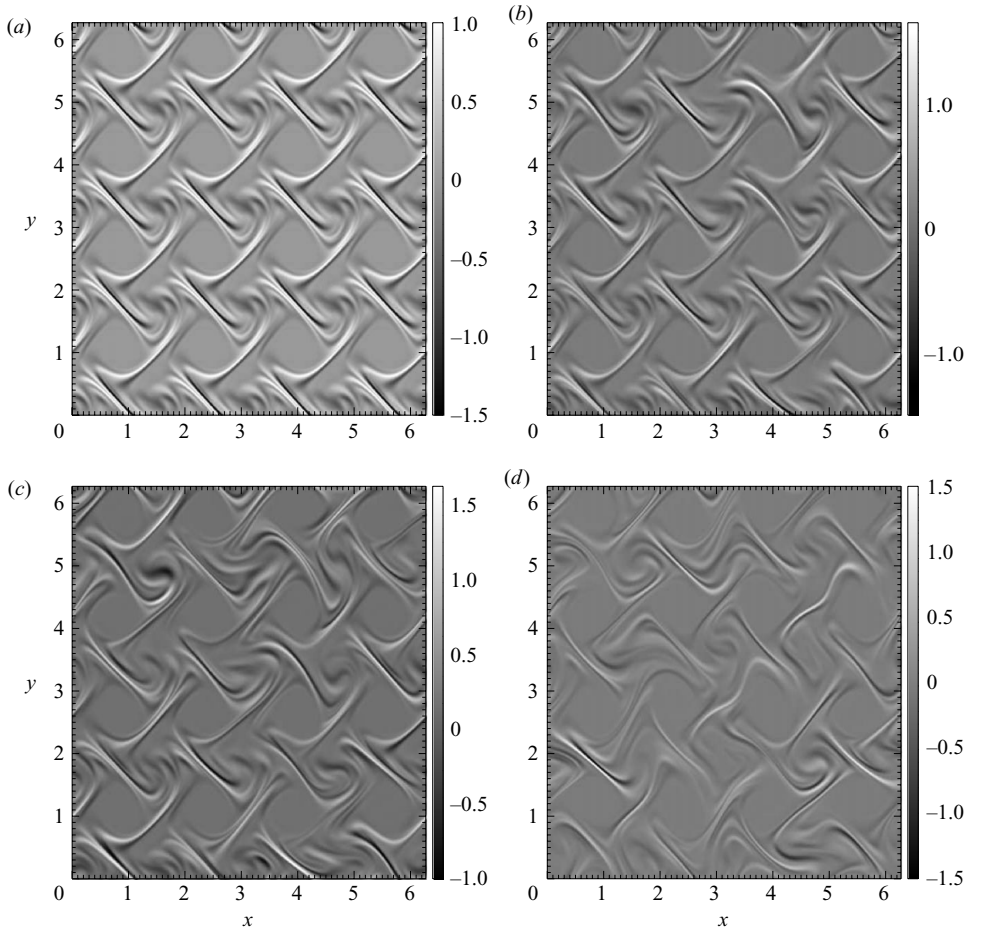

FIGURE 5. Snapshots of b_x in flow (3.4), normalised by its maximum value for $\boldsymbol{\phi} = \mathbf{0}$. (*a*) $\boldsymbol{\phi} = \mathbf{0}$, (*b*) $\boldsymbol{\phi} \in \mathcal{N}(0, 0.5)$, (*c*) $\boldsymbol{\phi} \in \mathcal{N}(0, 1)$ and (*d*) $\boldsymbol{\phi} \in \mathcal{U}([0, 2\pi])$.

We now consider the dependence of the α-effect on the magnetic Reynolds number, concentrating here on the behaviour of α_{11}. Figure 8 shows the dependence of α_{11} on Rm_k, normalized by the r.m.s. velocity, for $k = 4$ and $k = 16$ and for different phase distributions. For comparison, the dependence of α_{11} on Rm_k for the unperturbed flows is also shown.

For both flows and for $Rm_k \leqslant O(10)$, the value of α_{11} is affected little by the spatial decorrelations, whereas for higher values of Rm_k, α_{11} decreases substantially in magnitude as the spatial periodicity of the flows is perturbed. We also note that the Rm-dependence of α_{11} weakens as the flows are spatially decorrelated. This phenomenon is more obvious for flow (3.4) and is suggestive of α_{11} reaching an Rm-independent limit as Rm increases.

For flow (3.4), the values of α_{11} for $\boldsymbol{\phi} \in \mathcal{N}(0, 0.2)$ are very close to those for the unperturbed case, the phase differences being too small to affect the transport properties of the flow significantly. However, as the variance of the phase distribution increases, and also for a uniform distribution, $|\alpha_{11}|$ is markedly reduced and even reaches values very close to zero for $\boldsymbol{\phi} \in \mathcal{U}([0, 2\pi])$. This phenomenon is reinforced

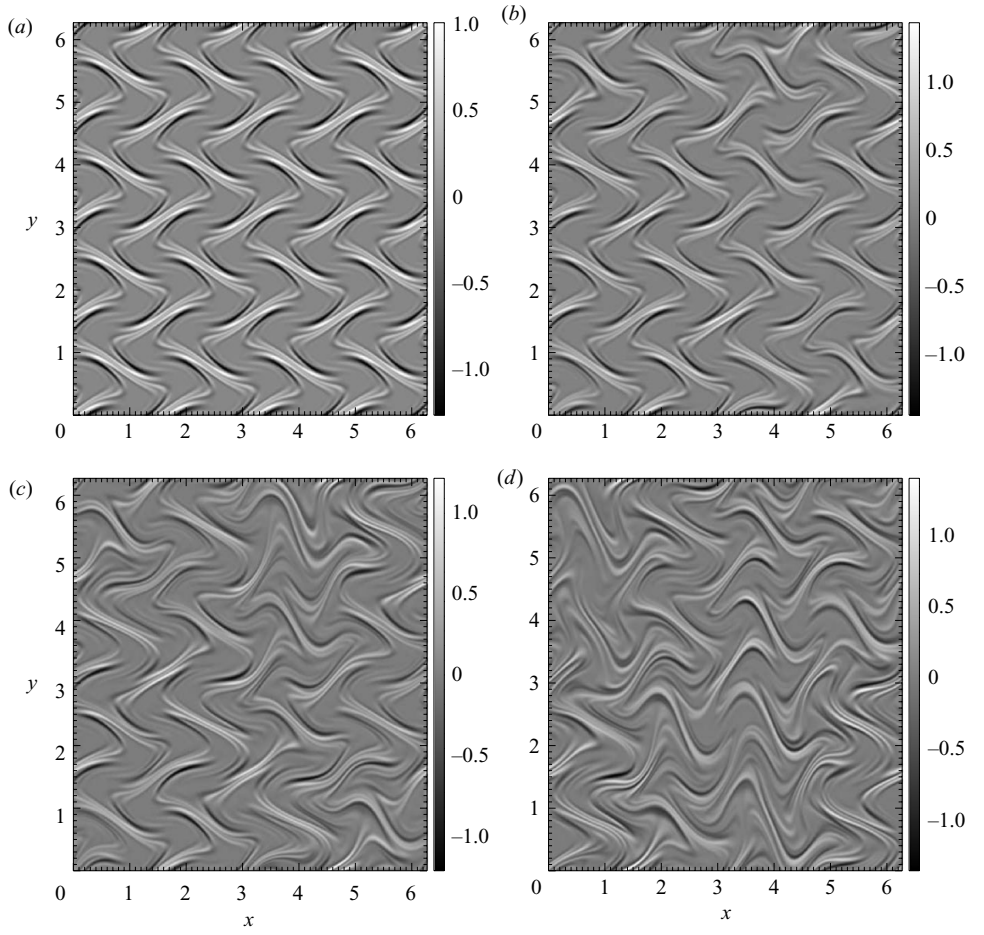

FIGURE 6. Snapshots of b_x in flow (3.5), normalised by its maximum value for $\boldsymbol{\phi} = \mathbf{0}$. (*a*) $\boldsymbol{\phi} = \mathbf{0}$, (*b*) $\boldsymbol{\phi} \in \mathcal{N}(0, 0.2)$, (*c*) $\boldsymbol{\phi} \in \mathcal{N}(0, 0.5)$ and (*d*) $\boldsymbol{\phi} \in \mathcal{U}([0, 2\pi])$.

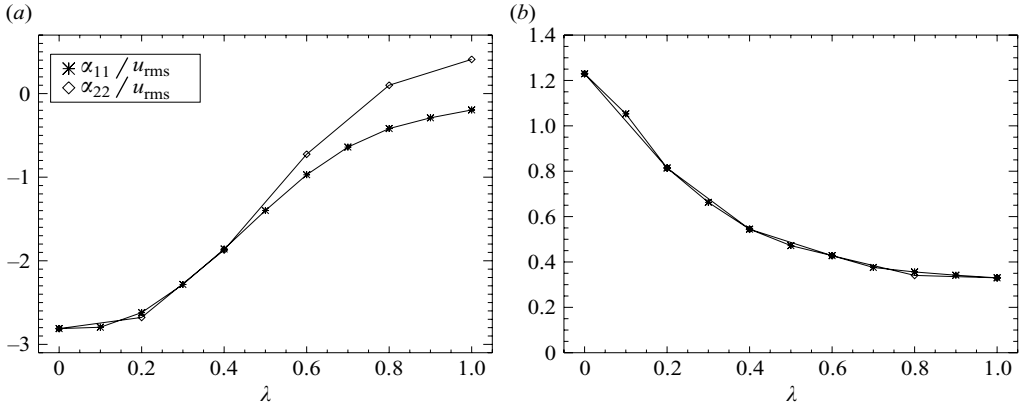

FIGURE 7. α_{11} and α_{22}, rescaled with the r.m.s. velocity, versus λ in (*a*) flow (3.4) and (b) flow (3.5); $Rm_k = 128$, $k = 16$, $\boldsymbol{\phi} \in \mathcal{N}(0, \lambda)$.

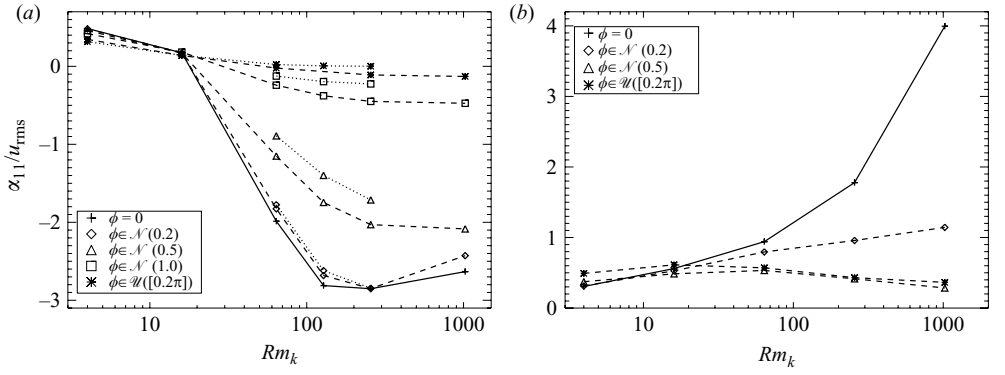

FIGURE 8. α_{11}, rescaled by the r.m.s. velocity, versus Rm_k in (a) flow (3.4) and (b) flow (3.5). Solid lines show the values of α in (a) the CP flow and (b) the MW+ flow. Dashed lines correspond to $k = 4$ and dotted lines to $k = 16$.

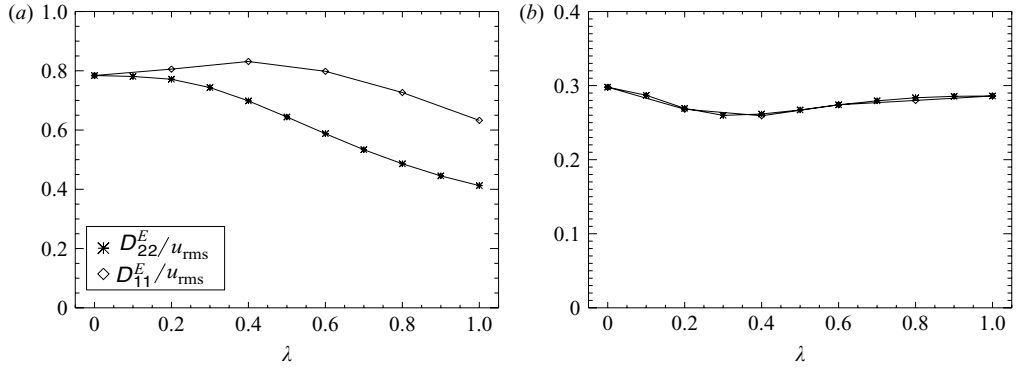

FIGURE 9. D^E_{22} and D^E_{11}, rescaled by the r.m.s. velocity, versus λ in (a) flow (3.4) and (b) flow (3.5); $Rm_k = 128$, $k = 16$, $\boldsymbol{\phi} \in \mathcal{N}(0, \lambda)$.

for larger values of k and, indeed, the values of $|\alpha_{11}|$ for $k = 16$ are mainly found below the corresponding values for $k = 4$.

For flow (3.5), figure 8(b) shows that in this case also, the modulus of α_{11} is reduced as the flow is spatially decorrelated. This effect is yet more dramatic here since even for $\boldsymbol{\phi} \in \mathcal{N}(0, 0.2)$, the magnitude of α_{11} is significantly smaller than its value in the MW+ flow as soon as $Rm \geqslant O(100)$. Furthermore, the results for $\boldsymbol{\phi} \in \mathcal{N}(0, 0.5)$ are very close to those for uniformly distributed random phases. This can be understood by inspection of figures 1 and 2; the streamlines of flow (3.5) are more dramatically affected by a small phase change than those of flow (3.4).

4.2. *The effective diffusivity*

In this subsection we explore, in an entirely analogous manner to that discussed in § 4.1, the influence of spatial decoherence on the effective diffusivity tensor $\boldsymbol{D}^E$. We first determine how the effective diffusivity varies as λ is increased at a fixed Rm. The results are shown in figure 9, for the same parameter values as in figure 7.

For flow (3.4), we observe a monotonic decrease of D^E_{22}; its normalized value for $\lambda = 1$ is approximately 50 % of that for $\lambda = 0$. The component D^E_{11}, which differs from D^E_{22} as soon as $\lambda > 0$, increases slightly as the flow becomes more spatially incoherent,

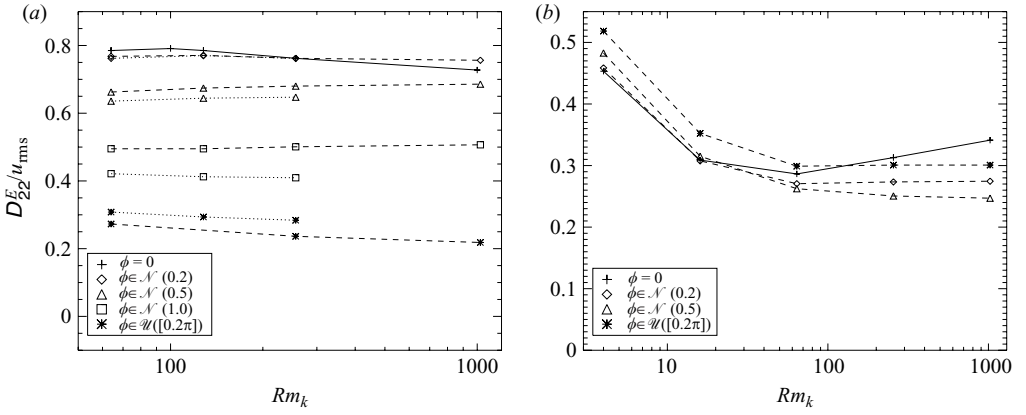

FIGURE 10. D_{22}^E, rescaled by the r.m.s. velocity, versus Rm_k in (a) flow (3.4) and (b) flow (3.5). Solid lines show the values of D^E in (a) the CP flow and (b) the MW+ flow. Dashed lines correspond to $k = 4$ and dotted lines to $k = 16$.

reaches a maximum for $\lambda \approx 0.4$, and subsequently decreases, always remaining higher than D_{22}^E.

For flow (3.5), D_{11}^E and D_{22}^E essentially coincide, varying little and non-monotonically with λ. Furthermore, and similarly to the α-effect, it appears that the effective diffusivity reaches a limit as $\lambda \to 1$, which also matches its value for $\boldsymbol{\phi} \in \mathscr{U}([0, 2\pi])$.

We now consider the dependence of the effective diffusivity on the magnetic Reynolds number, concentrating here on the behaviour of D_{22}^E. Figure 10 plots D_{22}^E, normalized by the r.m.s. velocity, as a function of Rm_k, for the same parameter regimes as used when determining α_{11} in figure 8. For both flows, the resulting curves show that for Rm_k high enough, the value of the effective diffusivity varies little with the magnetic Reynolds number, for all values of k and all phase distributions investigated. This is in agreement with the results of Biferale *et al.* (1995) who use a multiscale approach to determine the turbulent diffusivity in periodic flows with various degrees of Lagrangian chaos. For motions with strong Lagrangian chaos, scalar transport is controlled by chaotic advection and the turbulent diffusion attains a finite value, independent of the molecular diffusivity.

For flow (3.4), D_{22}^E is reduced as the velocity field becomes more decorrelated. Its value for $\boldsymbol{\phi} \in \mathscr{U}([0, 2\pi])$ corresponds to about a third of its value for the CP flow. Although this decrease is quite substantial, it is not as dramatic as that observed for the value of α_{11} with this flow. We also note that the values of D_{22}^E are not always lower for $k = 16$ than for $k = 4$.

The results for flow (3.5) seem qualitatively different. D_{22}^E keeps the same order of magnitude irrespective of the choice of phase distribution. For the lower values of Rm_k investigated (4, 16 and 64) the values of D_{22}^E for the perturbed flows can be higher than its value for the MW+ flow.

5. Discussion

We have considered two families of flows, based on those of Galloway & Proctor (1992) and Otani (1993), in order to examine systematically and quantitatively the role of spatial decorrelation on vector and scalar transport; more specifically we have examined the α-effect of mean field MHD and the mean diffusion of a passive

scalar. We have demonstrated that the α-effect is markedly affected by spatial phase modulations in the flows considered, with a pronounced reduction in the strength of the α-effect as the flows become more spatially decorrelated. Of significance is that velocity fields that are very similar in terms of their global properties, as determined, for example, by their helicity – a commonly used proxy for the α-effect – or by some measure of their chaotic properties, but which vary in their spatial coherence, can drive very different α-effects. By contrast, there is no such reduction in the effective diffusivity; indeed, the magnitude of the diffusivity can even increase as the spatial coherence is reduced. This is in keeping with the idea that the physics underlying the α-effect, which relies on the coherent summing of vector current elements, is altogether more subtle than that of turbulent scalar diffusion. It suggests that whereas it may be feasible to describe diffusion in terms of global quantities, via expressions such as (2.13), such an approach may be too simplistic for the $\boldsymbol{\alpha}$ tensor. Although our results do indicate that the α-effect becomes independent of λ once the flows are sufficiently decorrelated, thereby offering some hope of a theoretical result for sufficiently random flows, this should be tempered by the observation that the quantitative effect of spatial decorrelation for the two flows considered is different; the reduction in α for flow (3.4) is much more marked.

Although we believe that generic results can be extracted from our investigations, it would be remiss not to acknowledge the differences in the transport properties of the two flows. For example, it can be clearly seen in figure 10 that the turbulent diffusion of the CP flow is much more sensitive to spatial decorrelations than that of the MW+ flow. Such differences in the decorrelated flows are, perhaps, not too surprising given the differences in the basic correlated flows. They may however highlight a more fundamental issue, namely that in a turbulent flow possessing some underlying structure the transport properties may depend critically on the precise nature of this non-random ingredient.

The decrease in the α-effect is consistent with recent simulations of rotating convection in a layer with spatial periodicity in the horizontal directions (Hughes & Cattaneo 2008). These show that in small spatial domains the flow is ordered and thus, by periodicity, coherent; the resulting α-effect is readily determined and is comparable with the r.m.s. velocity of the convection. In larger domains, on the other hand, which can accommodate many convective cells, the spatial correlation is reduced and the α-effect is characterized by sizeable temporal fluctuations, leading to the necessity of a long time sequence in order even to calculate an average, and to a very small mean value. The issue of determining the transport coefficients in turbulent convection is however still far from being fully understood. For example, in the determination of α, although all simulations highlight the need for lengthy averaging, since the fluctuations dominate the mean, some yield a significant α-effect even in spatially extended domains (e.g. Giesecke, Ziegler & Rüdiger 2005; Ossendrijver, Stix & Brandenburg 2001). It is interesting to conjecture that this arises through greater spatial coherence of the flows.

We conclude by commenting on the differences between spatial and temporal decoherence within our models. In Courvoisier *et al.* (2006) temporal decorrelation was introduced via a new time scale. Although all cells act together, if the new time scale is sufficiently short then the influence of the spatial structure of the underlying flow is greatly reduced. By contrast, in the model discussed here, the means by which spatial decorrelations have been introduced implies that the structure of any individual cell is always felt, with any effects of disorder arising from phase shifts between neighbouring cells.

We thank the referees for their helpful comments on the paper and gratefully acknowledge financial support for this research from STFC. DWH is also grateful for the support of a Royal Society Leverhulme Senior Fellowship, during the tenure of which this work was completed.

Appendix. Derivation of expression (2.20)

The theorem of Zel'dovich (1957) (see also Diamond, Hughes & Kim 2005) is based on the evolution equation for the mean square potential $\overline{a^2}$ in the presence of an imposed mean gradient $\nabla\overline{A}$, which is given by (see (2.18))

$$\partial_t(a^2/2) + a\boldsymbol{u}\cdot\nabla a = Rm^{-1}\,a\nabla^2 a - a\boldsymbol{u}\cdot\nabla\overline{A}. \tag{A 1}$$

This may be rewritten as

$$\partial_t(a^2/2) = \nabla\cdot(Rm^{-1}a\nabla a - a^2\boldsymbol{u}/2) - Rm^{-1}(\nabla a)^2 - a\boldsymbol{u}\cdot\nabla\overline{A}. \tag{A 2}$$

Now we consider the case of space- and time-periodic flows and take the average of (A 2), using (3.7). The divergence term as well as the time derivative vanish, owing to the periodicities of $\boldsymbol{u}$ and a. This leads to the expression

$$0 = -Rm^{-1}\overline{(\nabla a)^2} - \overline{a\boldsymbol{u}}\cdot\nabla\overline{A}, \tag{A 3}$$

or, equivalently,

$$0 = -Rm^{-1}\overline{b_H^2} + (\mathbf{D}\cdot\nabla\overline{A})\cdot\nabla\overline{A}, \tag{A 4}$$

which gives (2.20).

REFERENCES

Biferale, L., Crisanti, A., Vergassola, M. & Vulpiani, A. 1995 Eddy diffusivities in scalar transport. *Phys. Fluids* **7**, 2725–2734.

Cattaneo, F. & Hughes, D. W. 2006 Dynamo action in a rotating convective layer. *J. Fluid Mech.* **553**, 401–418.

Cattaneo, F. & Hughes, D. W. 2009 Problems with kinematic mean field electrodynamics at high magnetic Reynolds numbers. *Mon. Not. R. Astr. Soc.* **395**, L48–L51.

Cattaneo, F., Hughes, D. W. & Proctor, M. R. E. 1988 Mean advection effects in turbulence. *Geophys. Astrophys. Fluid Dyn.* **41**, 335–342.

Cattaneo, F. & Tobias, S. M. 2005 Interaction between dynamos at different scales. *Phys. Fluids* **17**, 127105–127111.

Childress, S. & Gilbert, A. D. 1995 *Stretch, Twist, Fold: The Fast Dynamo*. Springer Verlag.

Childress, S. & Soward, A. M. 1989 Scalar transport and α-effect for a family of cat's-eye flows. *J. Fluid Mech.* **205**, 99–133.

Courvoisier, A. 2008 The α-effect in 2D fast dynamos. *Geophys. Astrophys. Fluid Dyn.* **102**, 217–243.

Courvoisier, A., Gilbert, A. D. & Ponty, Y. 2005 Dynamo action in flows with cat's eyes. *Geophys. Astrophys. Fluid Dyn.* **99**, 413–429.

Courvoisier, A., Hughes, D. W. & Tobias, S. M. 2006 α-effect in a family of chaotic flows. *Phys. Rev. Lett.* **96**. Id 034503.

Cowling, T. G. 1933 The magnetic field of sunspots. *Mon. Not. R. Astr. Soc.* **94**, 39–48.

Diamond, P. H., Hughes, D. W. & Kim, E. 2005 Self-consistent mean field electrodynamics in two and three dimensions. In *Fluid Dynamics and Dynamos in Astrophysics and Geophysics* (ed. A. M. Soward, C. A. Jones, D. W. Hughes & N. O. Weiss), pp. 145–192. CRC Press.

Galloway, D. J. & Proctor, M. R. E. 1992 Numerical calculations of fast dynamos for smooth velocity fields with realistic diffusion. *Nature* **356**, 691–693.

Gieseke, A., Ziegler, U. & Rüdiger, G. 2005 Geodynamo α-effect derived from box simulations of rotating magnetoconvection. *Phys. Earth Planet. Int.* **152**, 90–102.

Hughes, D. W. & Cattaneo, F. 2008 The α-effect in rotating convection: size matters. *J. Fluid Mech.* **594**, 445–461.

Knobloch, E. 1977 The diffusion of scalar and vector fields by homogeneous stationary turbulence. *J. Fluid Mech.* **83**, 129–140.

Kraichnan, R. H. 1976 Diffusion of passive scalar and magnetic fields by helical turbulence. *J. Fluid Mech.* **77**, 753–768.

Krause, F. & Rädler, K.-H. 1980 *Mean-Field Magnetohydrodynamics and Dynamo Theory*. Pergamon.

Majda, A. J. & Kramer, P. R. 1999 Simplified models for turbulent diffusion: theory, numerical modelling, and physical phenomena. *Phys. Rep.* **314**, 237–574.

Moffatt, H. K. 1978 *Magnetic Field Generation in Electrically Conducting Fluids*. Cambridge University Press.

Moffatt, H. K. 1983 Transport effects associated with turbulence with particular attention to the influence of helicity. *Rep. Prog. Phys.* **46**, 621–664.

Ossendrijver, M., Stix, M. & Brandenburg, A. 2001 Magnetoconvection and dynamo coefficients: dependence of the α-effect on rotation and magnetic field. *Astron. Astrophys.* **376**, 713–726.

Otani, N. F. 1993 A fast kinematic dynamo in time-dependent two-dimensional flows. *J. Fluid Mech.* **253**, 327–340.

Ottino, J. M. 1989 *The Kinematics of Mixing: Stretching, Chaos and Transport*. Cambridge University Press.

Plunian, F. & Rädler, K.-H. 2002 Harmonic and subharmonic solutions of the Roberts dynamo problem. Application to the Karlsruhe experiment. *Magnetohydrodynamics* **38**, 92–103.

Pouquet, A., Frisch, U. & Léorat, J. 1976 Strong MHD helical turbulence and the nonlinear dynamo effect. *J. Fluid Mech.* **88**, 1–16.

Rädler, K.-H. & Brandenburg, A. 2009 Mean-field effects in the Galloway-Proctor flow. *Mon. Not. R. Astr. Soc.* **393**, 113–125.

Roberts, G. O. 1970 Spatially periodic dynamos. *Phil. Trans. R. Soc. Lon.* A **266**, 535–558.

Roberts, P. H. 1994 Fundamentals of dynamo theory. In *Lectures on Solar and Planetary Dynamos* (ed. M. R. E. Proctor & A. D. Gilbert), pp. 1–58. Cambridge University Press.

Sturman, R., Ottino, J. M. & Wiggins, S. 2006 *Mathematical Foundations of Mixing: The Linked Twist Map as a Paradigm in Applications – Micro to Macro, Fluids to Solids*. Cambridge University Press.

Taylor, G. I. 1921 Diffusion by continuous movements. *Proc. Lon. Math. Soc.* A **20**, 196–211.

Zel'dovitch, Y. B. 1957 The magnetic field in the two-dimensional motion of a conductive fluid. *Sov. Phys. JETP* **4**, 460–462.